




Article

Investigation of the Parameters Influencing Baseline Ozone in the Western United States: A Statistical Modeling Approach

Matthew Ninneman ^{1,*} , Irina Petropavlovskikh ^{2,3}, Peter Effertz ^{2,3} , Duli Chand ⁴ and Daniel Jaffe ^{1,5} 

¹ School of Science, Technology, Engineering and Mathematics, University of Washington Bothell, 18115 Campus Way NE, Bothell, WA 98011, USA

² Cooperative Institute for Research in Environmental Sciences, 216 UCB, University of Colorado, Boulder, CO 80309, USA

³ National Oceanic and Atmospheric Administration Global Monitoring Laboratory, 325 Broadway, Boulder, CO 80305, USA

⁴ Atmospheric Sciences and Global Change Division, Pacific Northwest National Laboratory, P.O. Box 999, Richland, WA 99354, USA

⁵ Department of Atmospheric Sciences, University of Washington, 3920 Okanogan Lane, Seattle, WA 98195, USA

* Correspondence: mn77@uw.edu

Abstract: Ground-level ozone (O_3) is a key atmospheric gas that controls the oxidizing capacity of the atmosphere and has significant health and environmental implications. Due to ongoing reductions in the concentrations of O_3 precursors, it is important to assess the variables influencing baseline O_3 to inform pollution control strategies. This study uses a statistical model to characterize daily peak 8 h O_3 concentrations at the Mount Bachelor Observatory (MBO), a rural mountaintop research station in central Oregon, from 2006–2020. The model was constrained by seven predictive variables: year, day-of-year, relative humidity (RH), aerosol scattering, carbon monoxide (CO), water vapor (WV) mixing ratio, and tropopause pressure. RH, aerosol scattering, CO, and WV mixing ratio were measured at MBO, and tropopause pressure was measured via satellite. For the full 15-year period, the model represents 61% of the variance in daily peak 8 h O_3 , and all predictive variables have a statistically significant ($p < 0.05$) impact on daily peak 8 h O_3 concentrations. Our results show that daily peak 8 h O_3 concentrations at MBO are well-predicted by the model, thereby providing insight into what affects baseline O_3 levels at a rural site on the west coast of North America.

Keywords: ozone; baseline ozone; statistical model; generalized additive model



Citation: Ninneman, M.; Petropavlovskikh, I.; Effertz, P.; Chand, D.; Jaffe, D. Investigation of the Parameters Influencing Baseline Ozone in the Western United States: A Statistical Modeling Approach. *Atmosphere* **2022**, *13*, 1883. <https://doi.org/10.3390/atmos13111883>

Academic Editors: Xingwang Zhao, Junzhou He and Zhipeng Deng

Received: 20 October 2022

Accepted: 10 November 2022

Published: 11 November 2022

Publisher's Note: MDPI stays neutral with regard to jurisdictional claims in published maps and institutional affiliations.



Copyright: © 2022 by the authors. Licensee MDPI, Basel, Switzerland. This article is an open access article distributed under the terms and conditions of the Creative Commons Attribution (CC BY) license (<https://creativecommons.org/licenses/by/4.0/>).

1. Introduction

Ground-level ozone (O_3) production occurs due to photochemical reactions between oxides of nitrogen (NO_x = nitric oxide (NO) + nitrogen dioxide (NO_2)) and volatile organic compounds (VOCs). High concentrations of O_3 are harmful to human and ecosystem health [1–3]. Consequently, O_3 is subject to regulatory action by the U.S. Environmental Protection Agency (EPA). Compliance with the O_3 National Ambient Air Quality Standard (NAAQS) set by the U.S. EPA is achieved when the annual fourth-highest maximum daily 8 h average (MDA8) O_3 concentration is no more than 70 parts per billion (ppb), averaged over a three-year period [4]. Numerous studies have highlighted the successes and challenges of meeting this standard across the U.S. [5–8]. Due to the health and regulatory implications of surface O_3 , it is important to have a comprehensive understanding of the factors controlling O_3 levels.

One factor that affects ambient O_3 concentrations at surface U.S. sites is the amount of U.S. background O_3 (USBO), defined as the O_3 that would be present in the absence of U.S. anthropogenic emissions. However, since USBO cannot be observed directly, we instead refer to baseline O_3 , which is the O_3 concentration observed at a rural or remote site that has

not been influenced by recent, local emissions [9]. Previous work has investigated baseline O₃ concentrations throughout the U.S. [9–26]. For example, Ambrose et al. [25] found that baseline O₃ at the Mount Bachelor Observatory (MBO)—a rural mountaintop research station in central Oregon—was strongly influenced by long-range transport and upper tropospheric/lower stratospheric intrusions. In addition, Zhang and Jaffe [26] identified smoke and precursor emissions from wildfires as a source of baseline O₃ at MBO.

Baseline O₃ levels can have major implications for air quality management, especially in the western U.S. (WUS). In many parts of the WUS, mean seasonal baseline O₃ concentrations comprise up to 70% of the national O₃ standard [24,27,28], making it challenging for those areas to attain the O₃ NAAQS. These high baseline O₃ values are due in part to stratospheric intrusions [6,16], intercontinental transport of O₃ [17], and increased wildfire activity over the past two decades [9,29].

Although many previous studies have assessed baseline O₃ concentrations in the U.S., little has been done to examine the effect of individual meteorological and chemical parameters on baseline O₃ at rural high-elevation sites in the WUS. This is noteworthy for three reasons. First, such locations are far from major anthropogenic pollution sources. Second, such sites are frequently impacted by free tropospheric air. These characteristics make rural high-elevation sites well-suited for investigating what influences baseline O₃ concentrations. Third, as discussed above, baseline O₃ is a large fraction of the ambient O₃ for much of the WUS. Therefore, knowing which meteorological and chemical variables exert the greatest influence on baseline O₃ in the WUS is essential for creating pollution control strategies aimed at lowering O₃ levels in the region.

In the present study, we investigated the impact of several meteorological and chemical parameters on O₃ concentrations at MBO from 2006–2020 by using a machine learning/statistical model that is described in the next section. The goal of this work is to gain a better understanding of what affects baseline O₃ in the WUS.

2. Materials and Methods

The Mount Bachelor Observatory (MBO; 43.98° N, 121.69° W, 2764 m a.s.l.) is a rural mountaintop research station located in central Oregon that was established in 2004 [30]. Continuous measurements of O₃, carbon monoxide (CO), air temperature (T_{air}), barometric pressure (BP), relative humidity (RH), and other chemical and meteorological parameters have been made at MBO since its inception [25,31]. The MBO data have been used previously in a number of trend and model assessments [9,26,32–35]. Since MBO is a high-elevation site located far from major urban areas, it is an ideal site for examining the variables that affect baseline O₃ in the WUS.

In this study, hourly averaged data for several meteorological and chemical variables were used to investigate what influenced O₃ concentrations at MBO from 2006–2020. O₃ was measured using a Dasibi 1008-RS analyzer (Dasibi Environmental Corporation, Glendale, CA, USA) from 2006–2014 and an EcoTech Serinus 10 analyzer (EcoTech, Warren, RI, USA) from 2014–2020 [25,32,36]. CO was measured using a Thermo 48C-Trace Level Enhanced analyzer (Thermo Fisher Scientific, Waltham, MA, USA) from 2006–2012 and a Picarro G2502 Cavity Ring-Down Spectrometer (Picarro, Santa Clara, CA, USA) from 2012–2020 [25,32,37]. Aerosol scattering was measured using a TSI nephelometer (TSI Incorporated, Shoreview, MN, USA) [38–40]. Water vapor (WV) mixing ratios were calculated following the methodology of Bolton [41]. RH measurements were also included.

Figure 1 shows the diurnal variability in median O₃ concentrations for each season. Consistent with previous studies conducted at MBO [25,36,42], we generally see a daytime minimum and nighttime maximum in O₃ due to upslope flow during the day and downslope flow at night. This influenced how we chose to average the data, as discussed below.

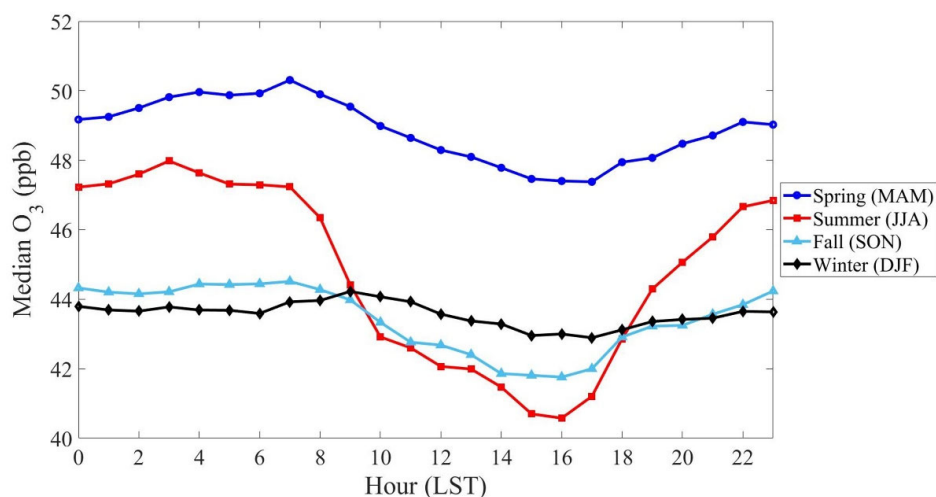


Figure 1. Diurnal variability in the median O₃ concentration at MBO for spring (MAM), summer (JJA), fall (SON), and winter (DJF) 2006–2020.

For this work, all hourly data were converted to running 8 h averages. Only 8 h averages calculated using at least six valid data points were included in the analysis. The 8 h averaged O₃ data were used to calculate the daily peak 8 h O₃ (hereafter referred to as peak 8 h O₃). To determine peak 8 h O₃, we considered a 24 h period starting at 12:00 LST. This was because O₃ concentrations at MBO typically exhibit a nighttime maximum and a daytime minimum (see Figure 1), consistent with other high-elevation sites [43–48]. As a result, we selected the 24 h window to start at 12:00 LST to allow for more variability in the timing of peak 8 h O₃. This 24 h window was also used to calculate the 8 h averages of all other hourly data. The 8 h averages of the other hourly data for the middle hour of the 8 h period when peak 8 h O₃ concentrations occurred were used in our analysis.

The 8 h averaged CO, aerosol scattering, RH, and WV mixing ratio data were used to help constrain a Generalized Additive Model (GAM), which was run using the “mgcv” package in R [49]. CO and aerosol scattering were used as model constraints because higher CO and aerosol scattering values correspond to more polluted airmasses, which likely contain higher concentrations of O₃ and its precursors. RH and WV mixing ratio were used to constrain the GAM because both are anticorrelated with O₃ in rural, low-NO_x environments [50,51]. Daily, 1° × 1° tropopause pressure data from the Atmospheric Infrared Sounder (AIRS) were used to further constrain the GAM [52]. Data were obtained for the ascending orbits, which move from south-to-north across the Equator at 13:30 local time [52]. Due to the 1° spatial resolution, the data are regionally representative. Daily regional tropopause pressure was included as a model constraint because peak 8 h O₃ at MBO is likely more influenced by lower-O₃ air originating from the boundary layer when the daily regional tropopause pressure is higher. In contrast, when the daily regional tropopause pressure is lower, peak 8 h O₃ at MBO is likely more influenced by higher-O₃ air originating from the free troposphere.

We also tested other variables as model inputs, but they were not part of the final model configuration. Specifically, we ran the Hybrid Single-Particle Lagrangian Integrated Trajectory (HYSPPLIT) model for each day using 1° × 1° Global Data Assimilation System (GDAS) meteorological data to calculate 24 h back trajectories for MBO. These were used to compute the direct transport distance and transport quadrant of airmasses. Even though these two variables help characterize the airmasses affecting MBO, they were not retained as model inputs because they were poorly correlated with peak 8 h O₃ (result not shown). Additionally, we tested observed, 8 h averaged T_{air} and BP as model constraints because high temperatures and stagnant conditions are often conducive to O₃ formation. However, neither T_{air} nor BP were retained as model inputs because we found that peak 8 h O₃ concentrations at MBO are weakly dependent on both parameters (results not shown).

GAMs are statistical models that use a sum of smooth functions of predictive variables to model a response variable [29,49,53,54]. Previous studies have used GAMs and other statistical models to meteorologically adjust trends in urban O₃ [55], examine the effect of wildfire smoke on urban O₃ concentrations [29,54], predict high-O₃ events in the Houston metropolitan area [56], and predict the impact of O₃ on net ecosystem production at a forested site in the Czech Republic [57]. However, to our knowledge, this is the first study to use a GAM to investigate what influences baseline O₃ levels in the WUS.

In this analysis, peak 8 h O₃ was the response variable, and the predictors are listed in Table 1. In addition to the model constraints discussed previously, “Year” and “day-of-year” were included as predictive variables due to the interannual and seasonal variability in the meteorological conditions impacting O₃ concentrations. One GAM simulation was done for the full 2006–2020 time period to assess the impact of each predictor on peak 8 h O₃ concentrations at MBO. Our approach for configuring the GAM was similar to the one used by Gong et al. [29]. For the smoothing function associated with each predictor, we used penalized cubic regression splines (CRSs) with 10 degrees of freedom to account for the complex, nonlinear relationship between peak 8 h O₃ and the predictive variables. Then, the seven selected predictors were added into the model one at a time to determine whether they decreased the Akaike information criterion (AIC) and increased the adjusted coefficient of determination (R²) [49,58,59]. Figure 2 shows that the AIC and adjusted R² decreased and increased, respectively, when the predictors were included in the model. Since the AIC continuously declined as each predictor was added, it is unlikely that our model is overfit.

Table 1. List of parameters used to constrain the Generalized Additive Model (GAM) for this study.

Data Source *	Parameter Number	Parameter Name (Unit)	Description
1	1	Year (unitless)	Year
1	2	DOY (unitless)	Day-of-year
2	3	RH_8h (%)	8 h average relative humidity
2	4	Scattering_8h (Mm ⁻¹)	8 h average aerosol scattering
2	5	CO_8h (ppb)	8 h average carbon monoxide
2	6	WV_8h (g kg ⁻¹)	8 h average water vapor mixing ratio
3	7	Tropopause_Pres (hPa)	Daily, satellite-derived regional tropopause pressure

* (1) Calculation, (2) MBO data archive, and (3) ascending orbit of the Atmospheric Infrared Sounder (AIRS).

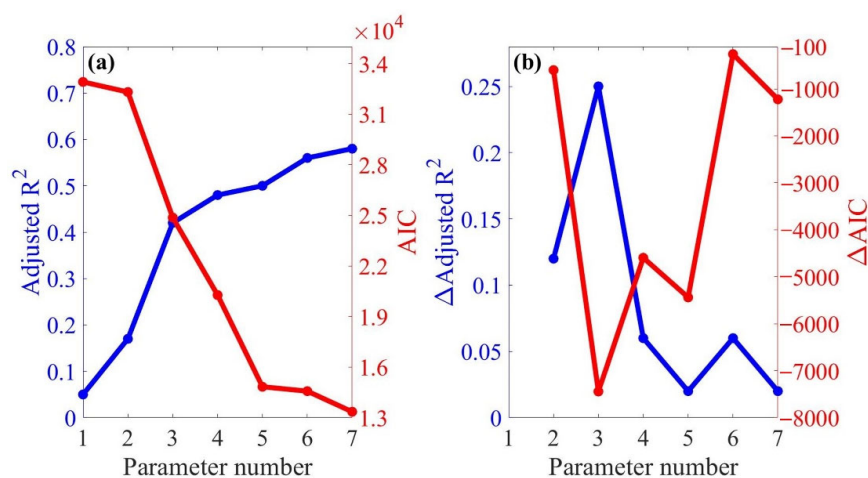


Figure 2. (a) Magnitude of adjusted R² and AIC with additional variables for MBO from 2006–2020. (b) Changes in adjusted R² and AIC with additional variables for MBO from 2006–2020. See Table 1 for the parameter names corresponding to the parameter numbers.

We further investigated baseline O_3 concentrations in the WUS from 2006–2020 by examining the seasonal variability in hourly and peak 8 h O_3 at MBO and O_3 measured via ozonesonde at Trinidad Head (THD), CA. THD is a rural coastal site in northern California; therefore, its O_3 profile measurements are characteristic of baseline O_3 values [21]. Since the average ambient pressure at MBO is approximately 730 hPa, THD O_3 profile data collected at the 680–780 hPa level during 798 balloon flights were included in our analysis so that the seasonality in O_3 at the two sites could be compared.

3. Results and Discussion

The seasonal variability in O_3 concentrations at MBO and THD (680–780 hPa) is shown in Figure 3. Median O_3 levels at MBO using all data ranged from 43 ppb in fall to 49 ppb in spring, median peak 8 h O_3 levels at MBO ranged from 46 ppb in winter to 53 ppb in spring, and median O_3 levels at THD ranged from 48 ppb in winter to 55 ppb in summer. These values are (1) in line with mean baseline O_3 concentrations of approximately 50 ppb reported for 15 other high-elevation sites in the WUS [16] and (2) about 61–79% of the 70 ppb O_3 NAAQS. The slightly lower seasonal concentrations of hourly O_3 at MBO were likely attributable to daytime upslope flow of boundary-layer air containing more moisture and less O_3 compared to free tropospheric air. Meanwhile, the comparable seasonal values of peak 8 h O_3 at MBO and O_3 at THD suggest that the two sites are affected by similar airmasses.

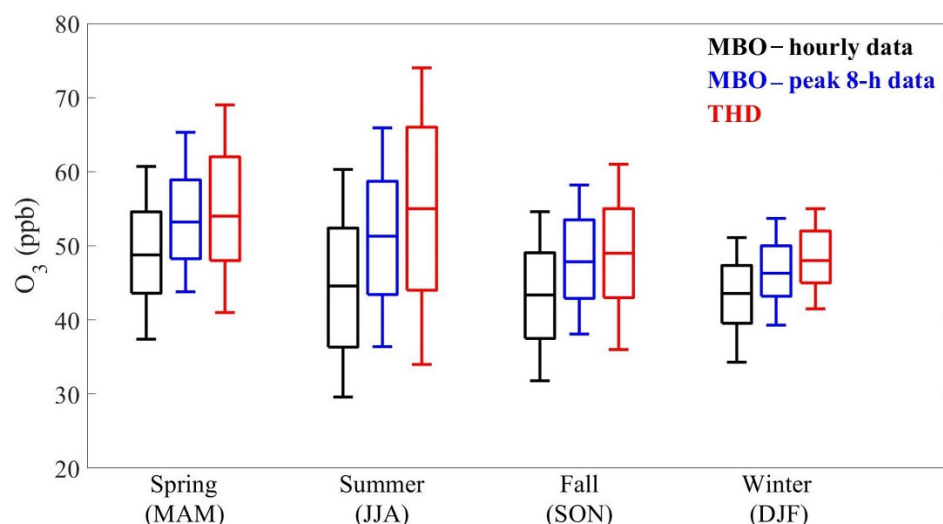


Figure 3. Seasonal O_3 concentrations at MBO and THD from 2006–2020. Hourly O_3 data were used to generate the MBO boxplots, and 680–780 hPa O_3 data collected via ozonesonde were used to generate the THD boxplots. The bottom and top whiskers denote the 10th and 90th percentile values, respectively, the central rectangles span the 25th percentile to the 75th percentile, and the horizontal lines within the central rectangles represent the median values.

Figure 4 compares the observed versus GAM-predicted peak 8 h O_3 at MBO from 2006–2020. Our model effectively predicted peak 8 h O_3 , with an adjusted R^2 of 0.61. All seven predictive variables had a statistically significant impact on peak 8 h O_3 levels ($p < 0.05$). The effects of RH, WV mixing ratio, aerosol scattering, CO, and daily regional tropopause pressure on peak 8 h O_3 are shown in Figures 5–9. Peak 8 h O_3 generally decreased with increasing RH and WV mixing ratio (Figures 5 and 6). Since MBO is in a rural, NO_x -sensitive environment, these relationships are likely due to increased removal of O_3 by hydrogen oxide radicals (HO_x = hydroxyl radical (OH) + hydroperoxyl radical (HO_2)) at higher RH and WV mixing ratios [51]. Aerosol scattering and CO values up to approximately 30 Mm^{-1} and 300 ppb, respectively, had a positive relationship with peak 8 h O_3 (Figures 7 and 8). This is consistent with higher levels of aerosol scattering, CO, O_3 , and O_3 precursors in more polluted airmasses. The response of peak 8 h O_3 to

aerosol scattering and CO values greater than about 30 Mm^{-1} and 300 ppb, respectively, is less clear because such high values are infrequently observed at MBO (see *x*-axes for Figures 7b and 8b). This led to the large model uncertainty at very high aerosol scattering and CO values. As shown in Figure 9, peak 8 h O_3 concentrations at MBO slightly decreased with increasing daily regional tropopause pressure. This is likely due to the lesser influence of free tropospheric air containing less moisture and more O_3 when daily regional tropopause pressure is higher.

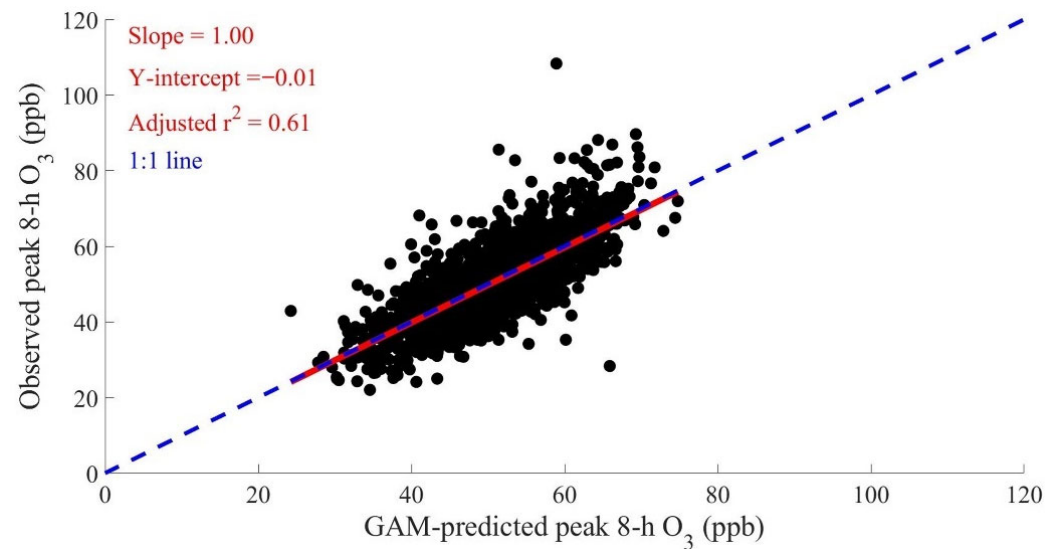


Figure 4. Observed versus GAM-predicted peak 8 h O_3 at MBO from 2006–2020. The solid red line and the dashed blue line are the trendline and 1:1 line, respectively.

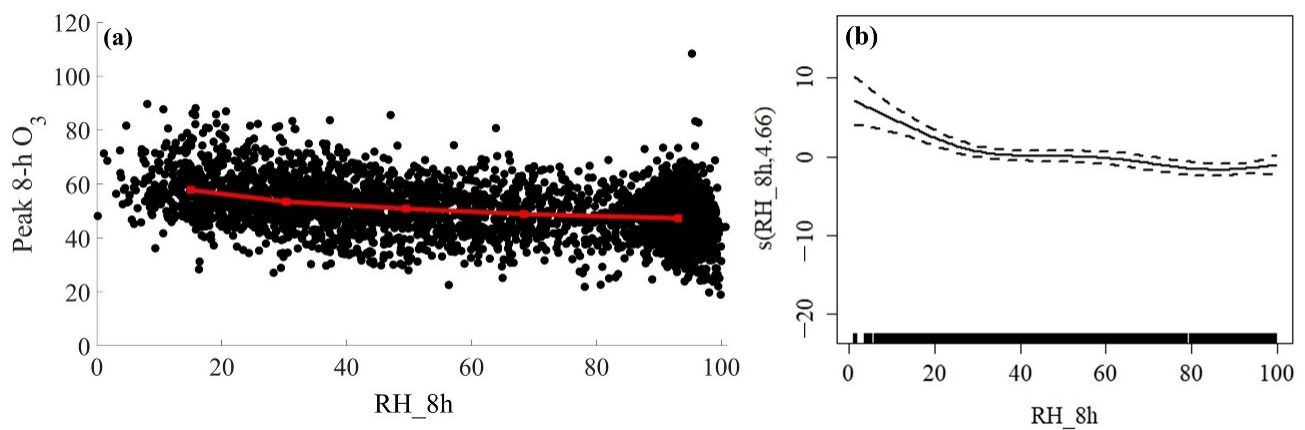


Figure 5. (a) Observed peak 8 h O_3 (ppb) versus observed 8 h average RH (%) at MBO from 2006–2020. The black dots show the individual data points, and the connected red squares show the median peak 8 h O_3 concentration, binned by 8 h average RH. The red squares are centered on the median 8 h average RH and the median peak 8 h O_3 concentration for each bin. (b) Partial response plot showing the effect of 8 h average RH (%) on model-predicted peak 8 h O_3 at MBO from 2006–2020. The tick marks on the *x*-axis denote the density of observed 8 h average RH values. The spline smoothing function for 8 h average RH is on the *y*-axis, with the label including its degrees of freedom (4.66). The solid line shows the smooth curve, and the dashed lines indicate 2 standard error bounds.

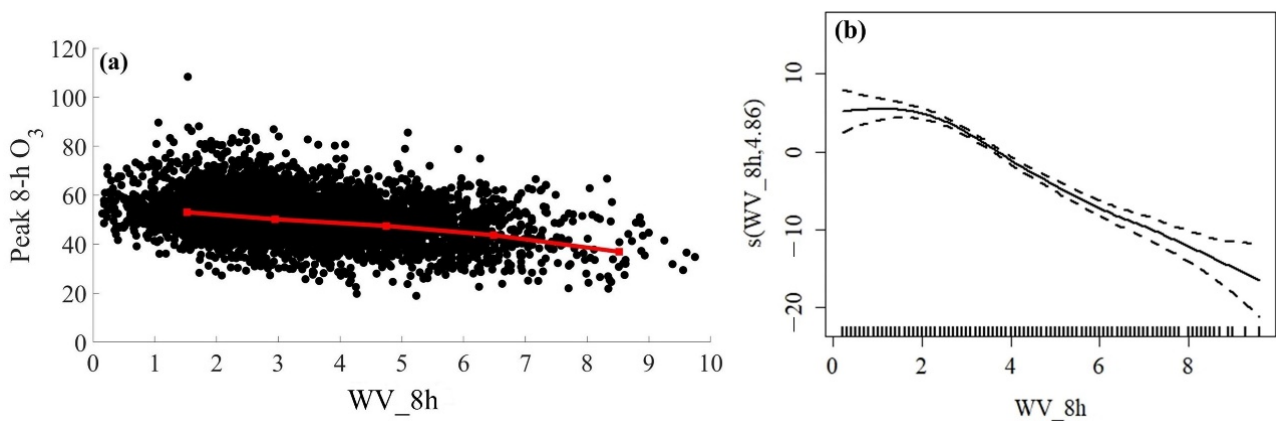


Figure 6. (a) Observed peak 8 h O₃ (ppb) versus observed 8 h average WV mixing ratio (g kg⁻¹) at MBO from 2006–2020. The black dots show the individual data points, and the connected red squares show the median peak 8 h O₃ concentration, binned by 8 h average WV mixing ratio. The red squares are centered on the median 8 h average WV mixing ratio and the median peak 8 h O₃ concentration for each bin. (b) Partial response plot showing the effect of 8 h average WV mixing ratio (g kg⁻¹) on model-predicted peak 8 h O₃ at MBO from 2006–2020. The tick marks on the x-axis denote the density of observed 8 h average WV mixing ratios. The spline smoothing function for 8 h average WV mixing ratio is on the y-axis, with the label including its degrees of freedom (4.86). The solid line shows the smooth curve, and the dashed lines indicate 2 standard error bounds.

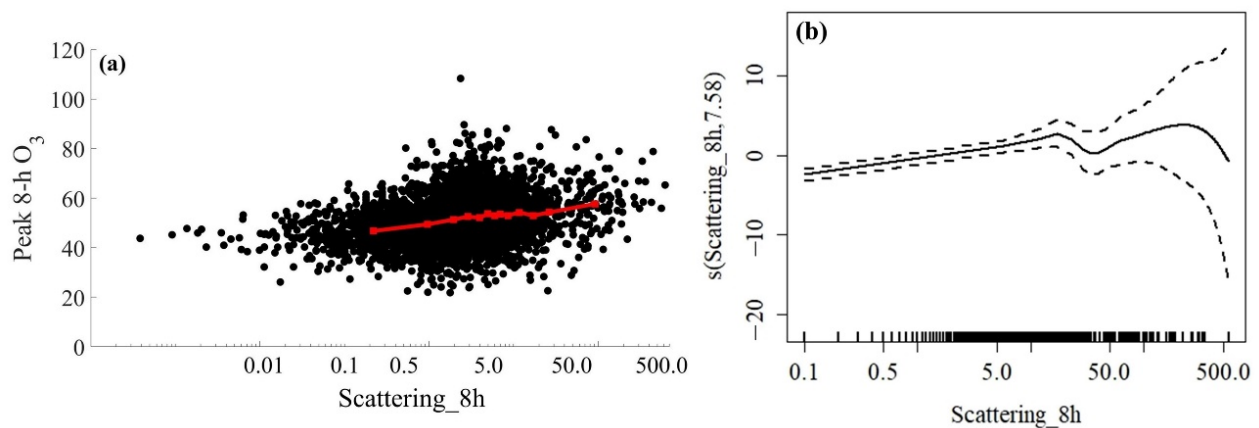


Figure 7. (a) Observed peak 8 h O₃ (ppb) versus observed 8 h average aerosol scattering (Mm⁻¹) at MBO from 2006–2020. The black dots show the individual data points, and the connected red squares show the median peak 8 h O₃ concentration, binned by 8 h average aerosol scattering. The red squares are centered on the median 8 h average aerosol scattering value and the median peak 8 h O₃ concentration for each bin. (b) Partial response plot showing the effect of 8 h average aerosol scattering (Mm⁻¹) on model-predicted peak 8 h O₃ at MBO from 2006–2020. The tick marks on the x-axis denote the density of observed 8 h average aerosol scattering values. The spline smoothing function for 8 h average aerosol scattering is on the y-axis, with the label including its degrees of freedom (7.58). The solid line shows the smooth curve, and the dashed lines indicate 2 standard error bounds. Note that the x-axes for panels (a) and (b) are plotted on a logarithmic scale.

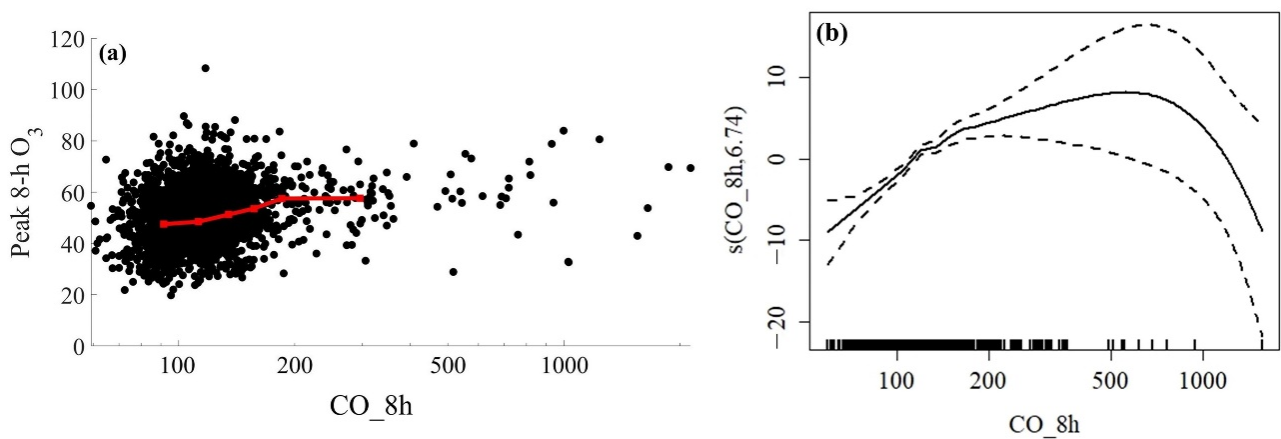


Figure 8. (a) Observed peak 8 h O_3 (ppb) versus observed 8 h average CO (ppb) at MBO from 2006–2020. The black dots show the individual data points, and the connected red squares show the median peak 8 h O_3 concentration, binned by 8 h average CO. The red squares are centered on the median 8 h average CO concentration and the median peak 8 h O_3 concentration for each bin. (b) Partial response plot showing the effect of 8 h average CO (ppb) on model-predicted peak 8 h O_3 at MBO from 2006–2020. The tick marks on the x -axis denote the density of observed 8 h average CO concentrations. The spline smoothing function for 8 h average CO is on the y -axis, with the label including its degrees of freedom (6.74). The solid line shows the smooth curve, and the dashed lines indicate 2 standard error bounds. Note that the x -axes for panels (a) and (b) are plotted on a logarithmic scale.

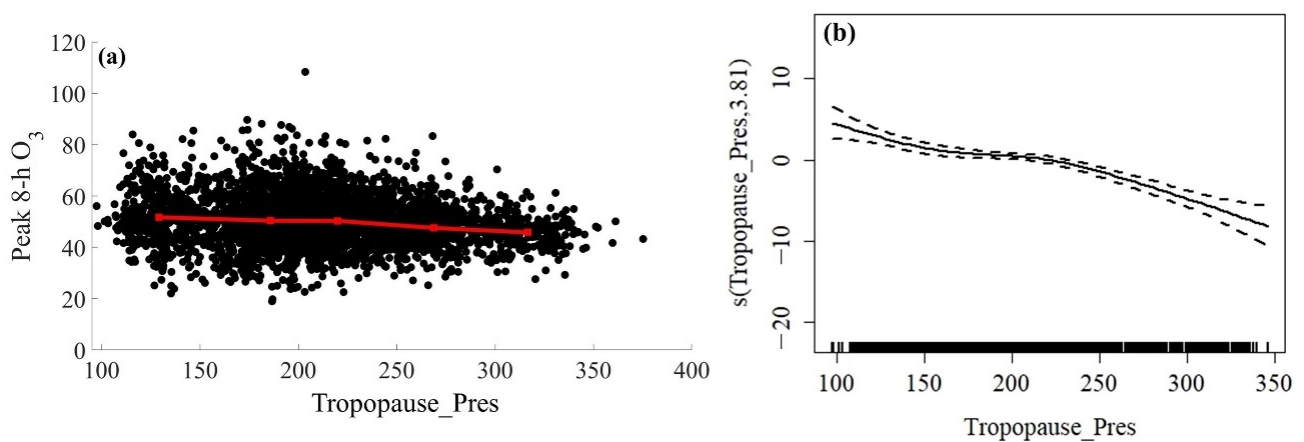


Figure 9. (a) Observed peak 8 h O_3 (ppb) versus observed daily regional tropopause pressure (hPa) for MBO from 2006–2020. The black dots show the individual data points, and the connected red squares show the median peak 8 h O_3 concentration, binned by daily regional tropopause pressure. The red squares are centered on the median daily regional tropopause pressure and the median peak 8 h O_3 concentration for each bin. (b) Partial response plot showing the effect of daily regional tropopause pressure (hPa) on model-predicted peak 8 h O_3 at MBO from 2006–2020. The tick marks on the x -axis denote the density of observed daily regional tropopause pressure values. The spline smoothing function for daily regional tropopause pressure is on the y -axis, with the label including its degrees of freedom (3.81). The solid line shows the smooth curve, and the dashed lines indicate 2 standard error bounds.

Figure 10 shows the residuals (observed peak 8 h O_3 —GAM-predicted peak 8 h O_3) for the full 15-year period, binned by GAM-predicted peak 8 h O_3 concentrations. Median residuals for all bins were close to 0 ppb, indicating that the seven-parameter model was unbiased across the O_3 distribution. This further demonstrates that our model was successful in predicting peak 8 h O_3 concentrations at MBO.

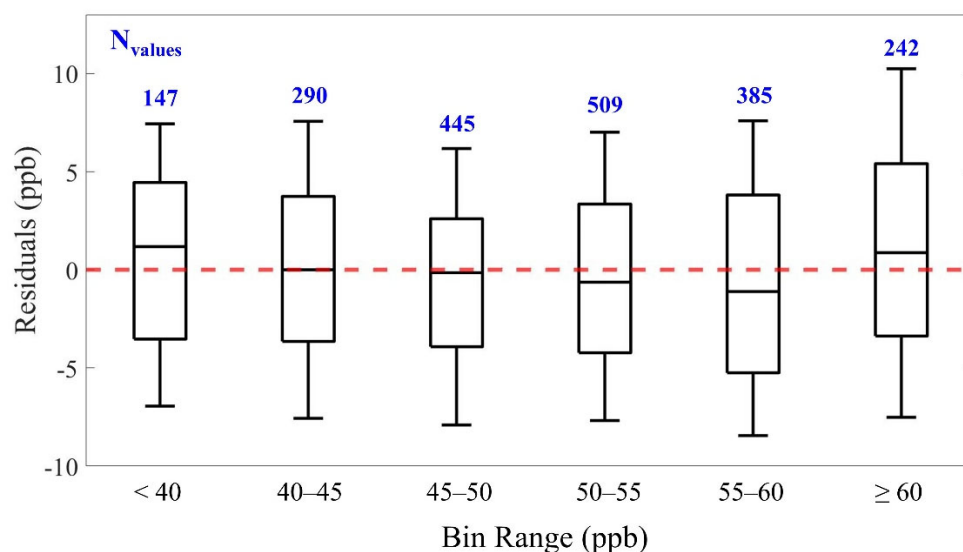


Figure 10. Residuals (observed peak 8 h O_3 – GAM-predicted peak 8 h O_3) at MBO from 2006–2020, binned by GAM-predicted peak 8 h O_3 concentrations. The dashed red line denotes 100% agreement between observed and GAM-predicted peak 8 h O_3 (i.e., residuals = 0 ppb). The components of each boxplot have the same meanings as in Figure 3.

It needs to be noted that ongoing climate change will impact the parameters affecting baseline O_3 in the WUS. For example, U.S. wildland fires have burned more than 3.2 million $ha\ y^{-1}$ in 10 of the past 18 years, and this increase in wildfire activity has primarily taken place in the WUS [60]. Climate-related factors such as higher summertime temperatures and drought have contributed to the increasing wildfire activity [61,62]. At MBO, more wildfires have led to higher aerosol optical thickness (AOT) values over the past decade, especially during summer and fall (Figure 11). Specifically, monthly AOT values were approximately 0.4 in August and September 2017, August 2018, and September 2020. Since wildfires are expected to increase in the future [63–65], such high monthly AOT values at MBO may become more common. This may lead to increased suppression of O_3 at MBO because high aerosol concentrations reduce solar radiation, which is not conducive to high O_3 levels [66]. However, increased O_3 suppression due to wildfires will only occur if MBO is increasingly impacted by fresh smoke plumes with very high aerosol loading. If increasing wildfires instead lead to an increase in the number of aged smoke plumes affecting MBO, then an increase in the number of high- O_3 days at MBO will likely occur. This is because aged smoke plumes have lower aerosol loading, and O_3 and aerosol scattering have a positive relationship at MBO, particularly at lower aerosol scattering values (Figure 7). Furthermore, higher temperatures and drier conditions during non-smoky periods in the WUS will likely lead to more high- O_3 days at MBO. This is because WV mixing ratios and O_3 are anticorrelated, and O_3 production and temperature are positively correlated [26,67]. Overall, due to (1) the effects of climate change on O_3 and (2) the impact of O_3 levels at MBO on downwind O_3 concentrations [68,69], future studies should consider reinvestigating the variables influencing O_3 concentrations at this rural site.

Two other items should also be the focus of future studies. First, future work should use a GAM to predict hourly O_3 concentrations at MBO. This will likely lead to an understanding of which variables have the greatest impact on the diurnal cycle of O_3 at MBO. Second, future studies should use a GAM constrained with surface observations of daily maximum O_3 and satellite observations of free tropospheric O_3 to predict daily maximum O_3 concentrations for MBO. For this analysis, the smoothing functions associated with the two predictive variables listed above will need to be penalized CRSs with two degrees of freedom. If this work is undertaken by future studies, the results may show how much daily maximum O_3 concentrations at MBO are affected by transport of free tropospheric

O₃. Such findings would further improve our understanding of what influences baseline O₃ concentrations in the WUS.

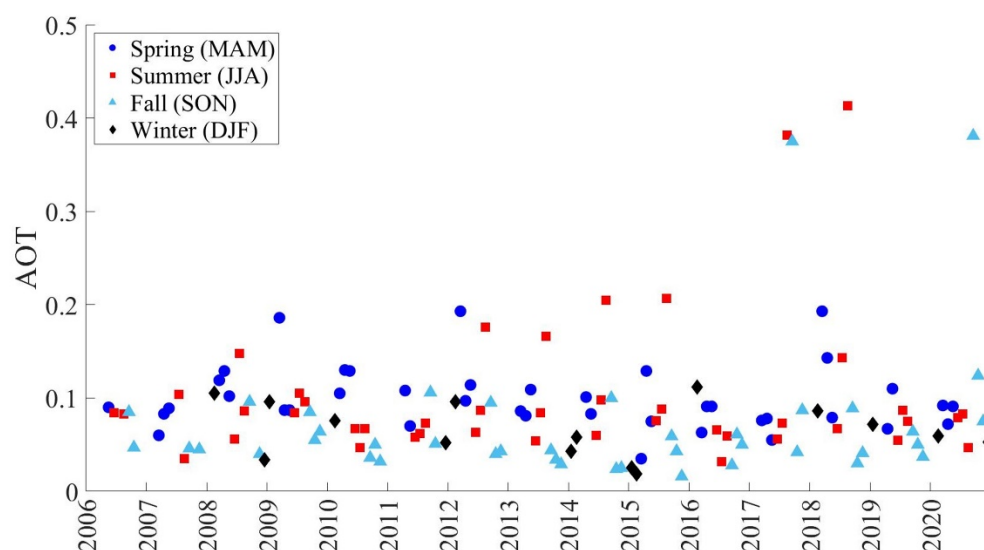


Figure 11. Monthly aerosol optical thickness (AOT) at MBO from 2006–2020. AOT data with 1° resolution were taken from the MODIS Aqua satellite.

4. Conclusions

This study examined the effects of several meteorological and chemical variables on peak 8 h O₃ at the Mount Bachelor Observatory (MBO) from 2006–2020. The analysis was completed using a Generalized Additive Model (GAM) constrained by seven parameters (Table 1). Over the 15-year period, our model successfully predicted the observed peak 8 h O₃, with an adjusted R² of 0.61. All predictive variables—year, day-of-year, daily regional tropopause pressure, and 8 h averaged relative humidity (RH), aerosol scattering, carbon monoxide (CO), and water vapor (WV) mixing ratio—significantly affected peak 8 h O₃ concentrations ($p < 0.05$). Our results show that peak 8 h O₃ levels at MBO were well-captured by the seven-parameter model. Therefore, since meeting the national O₃ standard continues to be challenging for much of the western U.S. (WUS), future work should consider using this study’s methodology to assess what influences baseline O₃ concentrations at other rural or remote sites in the region. This will help inform pollution control strategies aimed at reducing O₃ levels in the WUS.

Author Contributions: Conceptualization, M.N. and D.J.; methodology, M.N. and D.J.; software, M.N.; formal analysis, M.N.; investigation, M.N.; resources, I.P., P.E., D.C. and D.J.; data curation, D.C. and D.J.; writing—original draft preparation, M.N.; writing—review and editing, M.N., I.P., P.E., D.C. and D.J.; visualization, M.N.; supervision, D.J.; funding acquisition, I.P., P.E. and D.J. All authors have read and agreed to the published version of the manuscript.

Funding: This research was funded by the National Science Foundation, grant number AGS-1447832, and the National Oceanic and Atmospheric Administration, grant numbers RA-133R-16-SE-0758 and NA17OAR4320101. The APC was funded by the National Science Foundation, grant number AGS-1447832.

Institutional Review Board Statement: Not applicable.

Informed Consent Statement: Not applicable.

Data Availability Statement: Data for the Mount Bachelor Observatory are publicly available via the University of Washington’s Research Works Archive (https://digital.lib.washington.edu/researchworks/discover?scope=%2F&query=%22mt.+bachelor+observatory%22&submit=&filtertype_0=title&filter_relational_operator_0=contains&filter_0=data, accessed on 18 April 2022). Trinidad Head O₃ profile data for individual balloon flights can be found on the NOAA GML website (<https://gml.noaa.gov/dv/data/index.php?category=Ozone&type=Balloon&site=THD>, accessed on 14 July 2022).

The tropopause pressure data used in this study are publicly available via the NASA GES DISC database (<https://doi.org/10.5067/Aqua/AIRS/DATA303>, accessed on 20 September 2022). The aerosol optical thickness data from the MODIS Aqua satellite used in this study can be found on the MODIS Adaptive Processing System Services website (http://dx.doi.org/10.5067/MODIS/MYD08_M3.006, accessed on 20 June 2022). These data sources are cited in the References [52,70–72].

Acknowledgments: The authors thank Kai-Lan Chang of the Cooperative Institute for Research in Environmental Sciences at the University of Colorado for providing a single file that contained the Trinidad Head O₃ profile data.

Conflicts of Interest: The authors declare no conflict of interest. The funders had no role in the design of the study; in the collection, analyses, or interpretation of data; in the writing of the manuscript; or in the decision to publish the results.

References

1. Laurence, J.A. Ecological effects of ozone: Integrating exposure and response with ecosystem dynamics and function. *Environ. Sci. Policy* **1998**, *1*, 179–184. [CrossRef]
2. Lippmann, M. Health effects of tropospheric ozone. *Environ. Sci. Technol.* **1991**, *25*, 1954–1962. [CrossRef]
3. Zhang, J.; Wei, Y.; Fang, Z. Ozone Pollution: A Major Health Hazard Worldwide. *Front. Immunol.* **2019**, *10*, 2518. [CrossRef] [PubMed]
4. U.S. EPA. NAAQS Table. Criteria Air Pollutants. 2016. Available online: <https://www.epa.gov/criteria-air-pollutants/naaqs-table> (accessed on 30 June 2022).
5. Jaffe, D.A.; Ninneman, M.; Chan, H.C. NO_x and O₃ Trends at U.S. Non-Attainment Areas for 1995–2020: Influence of COVID-19 Reductions and Wildland Fires on Policy-Relevant Concentrations. *J. Geophys. Res. Atmos.* **2022**, *127*, e2021JD036385. [CrossRef] [PubMed]
6. Langford, A.O.; Alvarez, R.J., II; Brioude, J.; Fine, R.; Gustin, M.S.; Lin, M.Y.; Marchbanks, R.D.; Pierce, R.B.; Sandberg, S.P.; Senff, C.J.; et al. Entrainment of stratospheric air and Asian pollution by the convective boundary layer in the southwestern U.S. *J. Geophys. Res. Atmos.* **2017**, *122*, 1312–1337. [CrossRef]
7. Nussbaumer, C.M.; Cohen, R.C. The Role of Temperature and NO_x in Ozone Trends in the Los Angeles Basin. *Environ. Sci. Technol.* **2020**, *54*, 15652–15659. [CrossRef]
8. Simon, H.; Reff, A.; Wells, B.; Xing, J.; Frank, N. Ozone Trends Across the United States over a Period of Decreasing NO_x and VOC Emissions. *Environ. Sci. Technol.* **2015**, *49*, 186–195. [CrossRef]
9. Jaffe, D.A.; Cooper, O.R.; Fiore, A.M.; Henderson, B.H.; Tonnesen, G.S.; Russell, A.G.; Henze, D.K.; Langford, A.O.; Lin, M.; Moore, T. Scientific assessment of background ozone over the U.S.: Implications for air quality management. *Elem. Sci. Anthr.* **2018**, *6*, 56. [CrossRef]
10. Dolwick, P.; Akhtar, F.; Baker, K.R.; Possiel, N.; Simon, H.; Tonnesen, G. Comparison of background ozone estimates over the western United States based on two separate model methodologies. *Atmos. Environ.* **2015**, *109*, 282–296. [CrossRef]
11. Emery, C.; Jung, J.; Downey, N.; Johnson, J.; Jimenez, M.; Yarwood, G.; Morris, R. Regional and global modeling estimates of policy relevant background ozone over the United States. *Atmos. Environ.* **2012**, *47*, 206–217. [CrossRef]
12. Fiore, A.M.; Jacob, D.J.; Bey, I.; Yantosca, R.M.; Field, B.D.; Fusco, A.C.; Wilkinson, J.G. Background ozone over the United States in summer: Origin, trend, and contribution to pollution episodes. *J. Geophys. Res. Earth Surf.* **2002**, *107*, ACH-11-1–ACH 11-25. [CrossRef]
13. Fiore, A.; Jacob, D.J.; Liu, H.; Yantosca, R.M.; Fairlie, T.D.; Li, Q. Variability in surface ozone background over the United States: Implications for air quality policy. *J. Geophys. Res. Earth Surf.* **2003**, *108*, ACH-19-1–ACH-19-12. [CrossRef]
14. Fiore, A.M.; Oberman, J.T.; Lin, M.Y.; Zhang, L.; Clifton, O.E.; Jacob, D.J.; Naik, V.; Horowitz, L.W.; Pinto, J.P.; Milly, G.P. Estimating North American background ozone in U.S. surface air with two independent global models: Variability, uncertainties, and recommendations. *Atmos. Environ.* **2014**, *96*, 284–300. [CrossRef]
15. Lefohn, A.S.; Emery, C.; Shadwick, D.; Wernli, H.; Jung, J.; Oltmans, S.J. Estimates of background surface ozone concentrations in the United States based on model-derived source apportionment. *Atmos. Environ.* **2014**, *84*, 275–288. [CrossRef]
16. Lin, M.; Fiore, A.M.; Cooper, O.R.; Horowitz, L.W.; Langford, A.O.; Levy, H., II; Johnson, B.J.; Naik, V.; Oltmans, S.J.; Senff, C.J.; et al. Springtime high surface ozone events over the western United States: Quantifying the role of stratospheric intrusions. *J. Geophys. Res. Earth Surf.* **2012**, *117*, D00V22. [CrossRef]
17. Miyazaki, K.; Neu, J.L.; Osterman, G.; Bowman, K. Changes in US background ozone associated with the 2011 turnaround in Chinese NO_x emissions. *Environ. Res. Commun.* **2022**, *4*, 045003. [CrossRef]
18. Parrish, D.D.; Ennis, C.A. Estimating background contributions and US anthropogenic enhancements to maximum ozone concentrations in the northern US. *Atmos. Chem. Phys.* **2019**, *19*, 12587–12605. [CrossRef]
19. Parrish, D.D.; Young, L.M.; Newman, M.H.; Aikin, K.C.; Ryerson, T.B. Ozone Design Values in Southern California’s Air Basins: Temporal Evolution and U.S. Background Contribution. *J. Geophys. Res. Atmos.* **2017**, *122*, 11–166, 182. [CrossRef]
20. Parrish, D.D.; Faloon, I.C.; Derwent, R.G. Observational-based assessment of contributions to maximum ozone concentrations in the western United States. *J. Air Waste Manag. Assoc.* **2022**, *72*, 434–454. [CrossRef]

21. Stauffer, R.M.; Thompson, A.M.; Oltmans, S.J.; Johnson, B.J. Tropospheric ozonesonde profiles at long-term U.S. monitoring sites: 2. Links between Trinidad Head, CA, profile clusters and inland surface ozone measurements. *J. Geophys. Res. Atmos.* **2017**, *122*, 1261–1280. [[CrossRef](#)]
22. Wang, H.; Jacob, D.J.; Le Sager, P.; Streets, D.G.; Park, R.J.; Gilliland, A.B.; van Donkelaar, A. Surface ozone background in the United States: Canadian and Mexican pollution influences. *Atmos. Environ.* **2009**, *43*, 1310–1319. [[CrossRef](#)]
23. Yan, Q.; Wang, Y.; Cheng, Y.; Li, J. Summertime Clean-Background Ozone Concentrations Derived from Ozone Precursor Relationships are Lower than Previous Estimates in the Southeast United States. *Environ. Sci. Technol.* **2021**, *55*, 12852–12861. [[CrossRef](#)] [[PubMed](#)]
24. Zhang, L.; Jacob, D.J.; Downey, N.V.; Wood, D.A.; Blewitt, D.; Carouge, C.C.; van Donkelaar, A.; Jones, D.B.; Murray, L.; Wang, Y. Improved estimate of the policy-relevant background ozone in the United States using the GEOS-Chem global model with $1/2^\circ \times 2/3^\circ$ horizontal resolution over North America. *Atmos. Environ.* **2011**, *45*, 6769–6776. [[CrossRef](#)]
25. Ambrose, J.L.; Reidmiller, D.R.; Jaffe, D.A. Causes of high O₃ in the lower free troposphere over the Pacific Northwest as observed at the Mt. Bachelor Observatory. *Atmos. Environ.* **2011**, *45*, 5302–5315. [[CrossRef](#)]
26. Zhang, L.; Jaffe, D.A. Trends and sources of ozone and sub-micron aerosols at the Mt. Bachelor Observatory (MBO) during 2004–2015. *Atmos. Environ.* **2017**, *165*, 143–154. [[CrossRef](#)]
27. Jaffe, D.A.; Zhang, L. Meteorological anomalies lead to elevated O₃ in the western U.S. in June 2015. *Geophys. Res. Lett.* **2017**, *44*, 1990–1997. [[CrossRef](#)]
28. Jaffe, D.A.; Fiore, A.M.; Keating, T.J. Importance of background ozone for air quality management. *The Magazine for Environmental Managers*, 1 November 2020; 1–5. Available online: <https://pubs.awma.org/flip/EM-Nov-2020/jaffe.pdf> (accessed on 19 July 2022).
29. Gong, X.; Kaulfus, A.; Nair, U.; Jaffe, D.A. Quantifying O₃ Impacts in Urban Areas Due to Wildfires Using a Generalized Additive Model. *Environ. Sci. Technol.* **2017**, *51*, 13216–13223. [[CrossRef](#)]
30. Jaffe, D.; Prestbo, E.; Swartzendruber, P.; Weisspenzias, P.; Kato, S.; Takami, A.; Hatakeyama, S.; Kajii, Y. Export of atmospheric mercury from Asia. *Atmos. Environ.* **2005**, *39*, 3029–3038. [[CrossRef](#)]
31. Baylon, P.; Jaffe, D.A.; Hall, S.R.; Ullmann, K.; Alvarado, M.J.; Lefer, B.L. Impact of Biomass Burning Plumes on Photolysis Rates and Ozone Formation at the Mount Bachelor Observatory. *J. Geophys. Res. Atmos.* **2018**, *123*, 2272–2284. [[CrossRef](#)]
32. Gratz, L.E.; Jaffe, D.A.; Hee, J.R. Causes of increasing ozone and decreasing carbon monoxide in springtime at the Mt. Bachelor Observatory from 2004 to 2013. *Atmos. Environ.* **2015**, *109*, 323–330. [[CrossRef](#)]
33. Zhang, L.; Jacob, D.J.; Boersma, K.F.; Jaffe, D.A.; Olson, J.R.; Bowman, K.W.; Worden, J.R.; Thompson, A.M.; Avery, M.A.; Cohen, R.C.; et al. Transpacific transport of ozone pollution and the effect of recent Asian emission increases on air quality in North America: An integrated analysis using satellite, aircraft, ozonesonde, and surface observations. *Atmos. Chem. Phys.* **2008**, *8*, 6117–6136. [[CrossRef](#)]
34. Gaudel, A.; Cooper, O.R.; Ancellet, G.; Barret, B.; Boynard, A.; Burrows, J.P.; Clerbaux, C.; Coheur, P.-F.; Cuesta, J.; Cuevas, E.; et al. Tropospheric Ozone Assessment Report: Present-day distribution and trends of tropospheric ozone relevant to climate and global atmospheric chemistry model evaluation. *Elem. Sci. Anthr.* **2018**, *6*, 39. [[CrossRef](#)]
35. Qu, Z.; Henze, D.K.; Cooper, O.R.; Neu, J.L. Impacts of global NO_x inversions on NO₂ and ozone simulations. *Atmos. Chem. Phys.* **2020**, *20*, 13109–13130. [[CrossRef](#)]
36. Weiss-Penzias, P.; Jaffe, D.A.; Swartzendruber, P.; Dennison, J.B.; Chand, D.; Hafner, W.; Prestbo, E. Observations of Asian air pollution in the free troposphere at Mount Bachelor Observatory during the spring of 2004. *J. Geophys. Res. Earth Surf.* **2006**, *111*, D10304. [[CrossRef](#)]
37. Chen, H.; Karion, A.; Rella, C.W.; Winderlich, J.; Gerbig, C.; Filges, A.; Newberger, T.; Sweeney, C.; Tans, P.P. Accurate measurements of carbon monoxide in humid air using the cavity ring-down spectroscopy (CRDS) technique. *Atmos. Meas. Tech.* **2013**, *6*, 1031–1040. [[CrossRef](#)]
38. Briggs, N.L.; Jaffe, D.A.; Gao, H.; Hee, J.R.; Baylon, P.M.; Zhang, Q.; Zhou, S.; Collier, S.C.; Sampson, P.D.; Cary, R.A. Particulate Matter, Ozone, and Nitrogen Species in Aged Wildfire Plumes Observed at the Mount Bachelor Observatory. *Aerosol Air Qual. Res.* **2016**, *16*, 3075–3087. [[CrossRef](#)]
39. Zhou, S.; Collier, S.; Jaffe, D.A.; Briggs, N.L.; Hee, J.; Sedlacek, A.J., III; Kleinman, L.; Onasch, T.B.; Zhang, Q. Regional influence of wildfires on aerosol chemistry in the western US and insights into atmospheric aging of biomass burning organic aerosol. *Atmos. Chem. Phys.* **2017**, *17*, 2477–2493. [[CrossRef](#)]
40. Zhou, S.; Collier, S.; Jaffe, D.A.; Zhang, Q. Free tropospheric aerosols at the Mt. Bachelor Observatory: More oxidized and higher sulfate content compared to boundary layer aerosols. *Atmos. Chem. Phys.* **2019**, *19*, 1571–1585. [[CrossRef](#)]
41. Bolton, D. The Computation of Equivalent Potential Temperature. *Mon. Weather Rev.* **1980**, *108*, 1046–1053. [[CrossRef](#)]
42. Reidmiller, D.R.; Jaffe, D.A.; Fischer, E.V.; Finley, B. Nitrogen oxides in the boundary layer and free troposphere at the Mt. Bachelor Observatory. *Atmos. Chem. Phys.* **2010**, *10*, 6043–6062. [[CrossRef](#)]
43. Aneja, V.P.; Businger, S.; Li, Z.; Claiborn, C.S.; Murthy, A. Ozone climatology at high elevations in the southern Appalachians. *J. Geophys. Res. Earth Surf.* **1991**, *96*, 1007. [[CrossRef](#)]
44. Aneja, V.P.; Li, Z. Characterization of ozone at high elevation in the eastern United States: Trends, seasonal variations, and exposure. *J. Geophys. Res. Earth Surf.* **1992**, *97*, 9873–9888. [[CrossRef](#)]
45. Lefohn, A.S.; Shadwick, D.S.; Mohnen, V.A. The characterization of ozone concentrations at a select set of high-elevation sites in the eastern United States. *Environ. Pollut.* **1990**, *67*, 147–178. [[CrossRef](#)]

46. Lefohn, A.S.; Mohnen, V.A. The Characterization of Ozone, Sulfur Dioxide, and Nitrogen Dioxide for Selected Monitoring Sites in the Federal Republic of Germany. *J. Air Pollut. Control Assoc.* **1986**, *36*, 1329–1337. [[CrossRef](#)]
47. Mohnen, V.A.; Hogan, A.; Coffey, P. Ozone measurements in rural areas. *J. Geophys. Res. Earth Surf.* **1977**, *82*, 5889–5895. [[CrossRef](#)]
48. Naja, M.; Lal, S.; Chand, D. Diurnal and seasonal variabilities in surface ozone at a high altitude site Mt Abu (24.6°N, 72.7°E, 1680 m asl) in India. *Atmos. Environ.* **2003**, *37*, 4205–4215. [[CrossRef](#)]
49. Wood, S.N. *Generalized Additive Models: An Introduction with R*; Chapman & Hall/CRC: Boca Raton, FL, USA, 2006.
50. Kavassalis, S.C.; Murphy, J.G. Understanding ozone-meteorology correlations: A role for dry deposition. *Geophys. Res. Lett.* **2017**, *44*, 2922–2931. [[CrossRef](#)]
51. Lu, X.; Zhang, L.; Shen, L. Meteorology and Climate Influences on Tropospheric Ozone: A Review of Natural Sources, Chemistry, and Transport Patterns. *Curr. Pollut. Rep.* **2019**, *5*, 238–260. [[CrossRef](#)]
52. Teixeira, J. AIRS/Aqua L3 Daily Standard Physical Retrieval (AIRS-only) 1 degree × 1 degree V006. Available online: https://disc.gsfc.nasa.gov/datasets/AIRS3STD_006/summary (accessed on 20 September 2022).
53. Hastie, T.J.; Tibshirani, R.J. *Generalized Additive Models*; Chapman & Hall/CRC: Boca Raton, FL, USA, 1990.
54. McClure, C.D.; Jaffe, D.A. Investigation of high ozone events due to wildfire smoke in an urban area. *Atmos. Environ.* **2018**, *194*, 146–157. [[CrossRef](#)]
55. Camalier, L.; Cox, W.; Dolwick, P. The effects of meteorology on ozone in urban areas and their use in assessing ozone trends. *Atmos. Environ.* **2007**, *41*, 7127–7137. [[CrossRef](#)]
56. Sun, W.; Palazoglu, A.; Singh, A.; Zhang, H.; Wang, Q.; Zhao, Z.; Cao, D. Prediction of surface ozone episodes using clusters based generalized linear mixed effects models in Houston–Galveston–Brazoria area, Texas. *Atmos. Pollut. Res.* **2015**, *6*, 245–253. [[CrossRef](#)]
57. Jurán, S.; Edwards-Jonášová, M.; Cudlín, P.; Zapletal, M.; Šigut, L.; Grace, J.; Urban, O. Prediction of ozone effects on net ecosystem production of Norway spruce forest. *iForest-Biogeos. For.* **2018**, *11*, 743–750. [[CrossRef](#)]
58. Cavanaugh, J.E.; Neath, A.A. The Akaike information criterion: Background, derivation, properties, application, interpretation, and refinements. *WIREs Comput. Stat.* **2019**, *11*, e1460. [[CrossRef](#)]
59. CFI Team. Adjusted R-Squared. Available online: <https://corporatefinanceinstitute.com/resources/knowledge/other/adjusted-r-squared/> (accessed on 1 October 2022).
60. National Interagency Fire Center. Fire information: Statistics. Available online: <https://www.nifc.gov/fire-information/statistics> (accessed on 5 July 2022).
61. Aldersley, A.; Murray, S.J.; Cornell, S.E. Global and regional analysis of climate and human drivers of wildfire. *Sci. Total Environ.* **2011**, *409*, 3472–3481. [[CrossRef](#)] [[PubMed](#)]
62. Decker, Z.C.J.; Zarzana, K.J.; Coggon, M.; Min, K.-E.; Pollack, I.; Ryerson, T.B.; Peischl, J.; Edwards, P.; Dubé, W.P.; Markovic, M.Z.; et al. Nighttime Chemical Transformation in Biomass Burning Plumes: A Box Model Analysis Initialized with Aircraft Observations. *Environ. Sci. Technol.* **2019**, *53*, 2529–2538. [[CrossRef](#)]
63. Moritz, M.A.; Parisien, M.-A.; Batllori, E.; Krawchuk, M.A.; Van Dorn, J.; Ganz, D.J.; Hayhoe, K. Climate change and disruptions to global fire activity. *Ecosphere* **2012**, *3*, 1–22. [[CrossRef](#)]
64. Pechony, O.; Shindell, D.T. Driving forces of global wildfires over the past millennium and the forthcoming century. *Proc. Natl. Acad. Sci. USA* **2010**, *107*, 19167–19170. [[CrossRef](#)]
65. Val Martin, M.; Heald, C.L.; Lamarque, J.-F.; Tilmes, S.; Emmons, L.K.; Schichtel, B.A. How emissions, climate, and land use change will impact mid-century air quality over the United States: A focus on effects at national parks. *Atmos. Chem. Phys.* **2015**, *15*, 2805–2823. [[CrossRef](#)]
66. Buysse, C.E.; Kaulfus, A.; Nair, U.; Jaffe, D.A. Relationships between Particulate Matter, Ozone, and Nitrogen Oxides during Urban Smoke Events in the Western US. *Environ. Sci. Technol.* **2019**, *53*, 12519–12528. [[CrossRef](#)]
67. Sillman, S.; Samson, P.J. Impact of temperature on oxidant photochemistry in urban, polluted rural and remote environments. *J. Geophys. Res. Earth Surf.* **1995**, *100*, 11497–11508. [[CrossRef](#)]
68. Baylon, P.M.; Jaffe, D.A.; Pierce, R.B.; Gustin, M.S. Interannual Variability in Baseline Ozone and Its Relationship to Surface Ozone in the Western U.S. *Environ. Sci. Technol.* **2016**, *50*, 2994–3001. [[CrossRef](#)] [[PubMed](#)]
69. Wigder, N.L.; Jaffe, D.A.; Herron-Thorpe, F.L.; Vaughan, J.K. Influence of daily variations in baseline ozone on urban air quality in the United States Pacific Northwest. *J. Geophys. Res. Atmos.* **2013**, *118*, 3343–3354. [[CrossRef](#)]
70. Research Works Archive. Search: Mt. Bachelor Observatory. Available online: https://digital.lib.washington.edu/researchworks/discover?scope=%2F&query=%22mt.+bachelor+observatory%22&submit=&filtertype_0=title&filter_relational_operator_0=contains&filter_0=data (accessed on 18 April 2022).
71. NOAA GML. GML Data Finder. Available online: <https://gml.noaa.gov/dv/data/index.php?category=Ozone&type=Balloon&site=THD> (accessed on 14 July 2022).
72. Platnick, S.; Hubanks, P.; Meyer, K.; King, M.D. MODIS Atmosphere L3 Monthly Product (08_M3). Available online: http://dx.doi.org/10.5067/MODIS/MYD08_M3.006 (accessed on 20 June 2022).